RSC Advances

PAPER

View Article Online
View Journal | View Issue

Cite this: *RSC Adv.*, 2018, **8**, 38751

The influences of V and Gd dopants on the structures and electrical and magnetic properties of $PbPdO_2$ thin films

Hai Jia,[ab] Yanmin Yang,[ab] Weifeng Zheng,[ab] Jian-Min Zhang,*[ab] Shuiyuan Chen[ac] and Zhigao Huang *[ac]

Received 17th October 2018
Accepted 13th November 2018

DOI: 10.1039/c8ra08573k

rsc.li/rsc-advances

$PbPdO_2$, $PbPd_{0.9}V_{0.1}O_2$ and $PbPd_{0.9}Gd_{0.1}O_2$ thin films with body-centered orthorhombic structure were prepared by PLD technique, respectively. Their structures, magnetic and electrical properties were measured by XRD, SEM, AFM, EDS, XPS and VSM, respectively. The experimental results indicate that the three samples all have the preferred orientation of (002), and room temperature ferromagnetism. From EDS and XPS results, we can deduce that there exist Pb vacancies in the three samples. Meanwhile, the valence states for Pb, Pd, O, Gd and V ions were found to be 2+, 2+, 2−, 3+ and mixed 4+ and 5+, respectively. It was also found that the magnetic moments of $PbPdO_2$ and $PbPd_{0.9}Gd_{0.1}O_2$ are least and largest, respectively. Moreover, the electrical characteristics analysis indicates that the electrical resistivity is enhanced by V ion substitution, but reduced by Gd ion substitution. In addition, the significant insulator–metal transition temperatures of $PbPdO_2$, $PbPd_{0.9}V_{0.1}O_2$ and $PbPd_{0.9}Gd_{0.1}O_2$ were found to be about 385 K, 390 K and 430 K, respectively. Finally, according to the experimental facts of Pb vacancies in the three samples, the first-principles calculated models containing Pb vacancies were established. The calculated results explain well the magnetic origin of $PbPdO_2$, and V and Gd doping roles on its electrical and magnetic properties.

Introduction

Materials with a zero or small band gap (such as HgCdTe, HgZnSe, $PbPdO_2$, graphene, MoS_2 and topological insulators) have attracted increasing attention due to their intriguing physical properties.[1] $PbPdO_2$ was found to be a zero band gap semiconductor; it is very sensitive to the temperature, pressure and magnetic field.[2–4] Having many novel physical properties, the doped $PbPdO_2$ materials can hopefully be used in spintronics, electronics, optics, sensors and energy storage.[1] As early as 2005, Ozawa *et al.* synthesized $PbPdO_2$ single phase polycrystal samples by solid phase reaction.[2] The electrical, magnetic and thermoelectric properties were measured. A metal–insulator transition at about 90 K and p-type carriers were observed. In 2008, Wang proposed at first that Co-doped $PbPdO_2$ is a zero-spin gapless semiconductor (SGS) based on band structure calculations.[3] Then, Wang *et al.* prepared Co-doped $PbPdO_2$ thin films by pulsed laser deposition (PLD), and studied the effects of current and magnetic field on the resistivity in the thin film.[4] Both colossal electroresistance (CER) and giant magnetoresistance (GMR) were observed. Wang's pioneering research led to a series of experimental and theoretical studies of $PbPdO_2$. In the past few years, many researchers followed behind and studied theoretically and experimentally the microstructures, transport and magnetic properties of $PbPdO_2$ doped with different transition metal elements (such as Mn, Co, Cu, Zn, *etc.*).[5–13] Su *et al.* prepared single phase $PbPd_{0.81}Co_{0.19}O_2$ thin films by sol–gel spin coating and oxidation treatment.[5] It was found that the metal–insulator transition temperature of $PbPd_{0.81}Co_{0.19}O_2$ film is 358 K, which is markedly higher than 90 K. Choo *et al.* prepared $PbPdO_2$ and Pb (Pd, Co) O_2 thin films oriented along the (020) direction by PLD, and studied *ex situ* annealing effects on the surface morphology, electrical and magnetic properties.[6,7] They found that, the electrical conduction was improved for $PbPdO_2$ film by annealing, which can be well explained by the reduction of lattice imperfections of PdO droplets and Pd or O deficiencies. It is suggested that the hybridization between the Pd 4d and O 2p bands plays key role. Lee *et al.* studied the physical properties tuned by magnetic and nonmagnetic ion substitutions (Zn and Cu), found that chemical dopants play an important role.[9] When Pd in $PbPdO_2$ is substituted by Zn ($3d^{10}$), the electrical resistivity decreases and the magnetic properties are not changed to

[a]*College of Physics and Energy, Fujian Normal University, Fujian Provincial Key Laboratory of Quantum Manipulation and New Energy Materials, Fuzhou, 350117, China. E-mail: jmzhang@fjnu.edu.cn; zghuang@fjnu.edu.cn*

[b]*Fujian Provincial Engineering Technical Research Centre of Solar-Energy Conversion and Stored Energy, Fuzhou, 350117, China*

[c]*Fujian Provincial Collaborative Innovation Center for Optoelectronic Semiconductors and Efficient Devices, Xiamen, 361005, China*

remain diamagnetic. However, by substituting Cu^{2+} ($3d^9$) with $S = 1/2$, the electrical resistivity increases and the magnetization shows paramagnetic behavior.

In this paper, 3d transition element V and rare earth ferromagnetic element Gd were chosen as dopant ions. Why V and Gd dopants are considered? V is also 3d transition metal, and its properties are similar to those of Mn. And Gd is unique rare earth metal with room temperature magnetism. The $PbPdO_2$, $PbPd_{0.9}V_{0.1}O_2$ and $PbPd_{0.9}Gd_{0.1}O_2$ films were prepared using PLD technique. The structures, ion valence states, magnetic and electrical properties of the three samples were measured. The experimental results indicate that, $PbPdO_2$, $PbPd_{0.9}V_{0.1}O_2$ and $PbPd_{0.9}Gd_{0.1}O_2$ films have (002) preferred orientation and room temperature ferromagnetism. Both V and Gd dopants can evidently enhance the magnetic moment of $PbPdO_2$. Moreover, $PbPdO_2$ and $PbPd_{0.9}V_{0.1}O_2$ have about 390 K insulator–metal transition temperature, while $PbPb_{0.9}Gd_{0.1}O_2$ has a larger insulator–metal transition temperature with 430 K. At last, V dopant has the conductivity of $PbPdO_2$ increase, but Gd dopant makes the conductivity of $PbPdO_2$ to decrease. In addition, the calculated results based on density functional theory (DFT) were used to explain the experimental facts.

Experimental and first-principles calculation

At first, $PbPdO_2$, $PbPd_{0.9}V_{0.1}O_2$ and $PbPd_{0.9}Gd_{0.1}O_2$ nanoparticles were prepared by sol–gel method. $Pb(NO_3)_2$ (99.99%), $Pd(NO_3)_2$ (99.99%), $V(NO_3)_2$ (99.9%) and $Gd(NO_3)_3 \cdot 6H_2O$ (99.99%) were used as raw materials. The chelating agent and solvent were citric acid monohydrate ($C_6H_8O_7 \cdot H_2O$ 99.5%) and deionized water, respectively. In order to supplement the volatilization of Pb in the process of the heating treatment, an additional 5 mol% $Pb(NO_3)_2$ was used. Secondly, the $PbPdO_2$, $PbPd_{0.9}V_{0.1}O_2$ and $PbPd_{0.9}Gd_{0.1}O_2$ cylinder bulk sheets were synthesized by using their nanoparticles, respectively. $PbPdO_2$, $PbPd_{0.9}V_{0.1}O_2$ and $PbPd_{0.9}Gd_{0.1}O_2$ thin films were deposited on (100) oriented MgO single crystal substrate using PLD technique. The substrate temperature was 550 °C. A KrF excimer laser with wavelength of 248 nm was used as the energy source for target ablation. The energy and repetition rate of laser were chosen as about 250 mJ and 1 Hz, and the deposited time was 60 min. The samples were deposited at different O_2 ambient pressure and the initial vacuum condition of the chamber reached 10^{-6} torr. After deposition, the samples were *ex situ* annealed in air at 650 °C.

X-ray diffraction (XRD) patterns of $PbPdO_2$, $PbPd_{0.9}V_{0.1}O_2$ and $PbPd_{0.9}Gd_{0.1}O_2$ thin films were obtained by Rigaku Mini-Flex II (CuK_α, $\lambda = 0.15418$ nm). X-ray photoelectron spectra (XPS) were measured by using Thermo Fisher ESCALAB250Xi. The morphologies of the films were observed by Hitachi SU-8010 Scanning Electron Microscopy (SEM) and atomic force microscopy (AFM, Bruker Dimension), and the elements of the samples were analyzed by EDS. The electronic properties were measured by KEITHLEY 4200-SCS and HALL8686 semiconductor characterization system. The magnetic properties were measured by VersaLab (VSM) of Quantum Design.

Our DFT calculations were performed by Vienna ab initio simulation package (VASP)[14] with projected-augmented-wave (PAW) potential.[15] The functional of Perdew–Burke–Ernzerhof generalized gradient approximation (GGA-PBE)[16,17] were used in the all calculations. We choose a $PbPdO_2$ (002) film with the experimental lattice constants of $a = 9.4547$ Å, $b = 5.4597$ Å, $c = 4.6605$ Å. The adjacent atomic slabs were decoupled by using a vacuum layer of 15 Å. The cutoff energy was set at 550 eV. A $6 \times 8 \times 4$ Monkhorst *k*-point mesh was adopted for $2 \times 2 \times 1$ $PbPdO_2$ (002) film supercells. The on-site Hubbard *U* was included in the strong correlation elements Pd, Gd and V. All the atoms were fully relaxed until the residual forces on each atom are less than 0.02 eV $Å^{-1}$.

Results and discussion

Fig. 1(a) shows the XRD patterns of $PbPdO_2$, $PbPd_{0.9}V_{0.1}O_2$ and $PbPd_{0.9}Gd_{0.1}O_2$, film. In order to distinguish weaker peak, the log intensity as a function of 2θ was present in Fig. 1(b). From Fig. 1(a), it is found that $PbPdO_2$, $PbPd_{0.9}V_{0.1}O_2$ and $PbPd_{0.9}Gd_{0.1}O_2$ are mainly single-phase with body-centered orthorhombic structure with the standard PDF (No. 38-1357). The diffraction peaks observed at $2\theta = 31.52°$ and $2\theta = 38.60°$ are corresponding to (211) and (002) of $PbPdO_2$ phase, respectively. $PbPdO_2$, $PbPd_{0.9}V_{0.1}O_2$ and $PbPd_{0.9}Gd_{0.1}O_2$ films have all (002) preferred direction. V and Gd dopants do not change the crystal structure. Moreover, under log enlargement, four very weak peaks at $2\theta \approx 28.5°$, 30.0°, 32.5° and 33.7° were observed in $PbPd_{0.9}V_{0.1}O_2$ and $PbPd_{0.9}Gd_{0.1}O_2$ films, which means that there may exist very little impurity phases induced by the V and Gd dopants. By analyzing weak additional peaks, we find that, for $PbPdO_2$, there does hardly exist the additional peaks; for $PbPd_{0.9}V_{0.1}O_2$, the additional peaks are very weak, and they may correspond PdO phase; for $PbPd_{0.9}Gd_{0.1}O_2$, the additional peaks correspond Gd_2O_3 phase with paramagnetism. When the deposition time is short and the thickness of the sample is thin, there is a lattice mismatch between the substrate and $PbPdO_2$ thin film. The lattice constant *c* of $PbPdO_2$ (002) film is 4.6605 Å, while the lattice constant *a* of Mg (001) is 4.2112 Å. $PbPdO_2$ (002) films with $c = 4.6605$ Å can be grew on the MgO (001) substrate with $a = 4.2112$ Å because of little lattice mismatch (+9.7%). The detailed discussion can be found in our previous work.[11] So, the

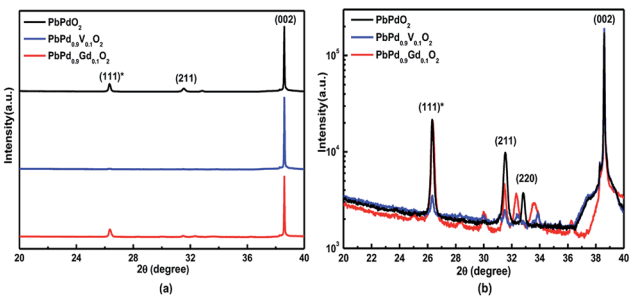

Fig. 1 XRD patterns of $PbPdO_2$, $PbPd_{0.9}V_{0.1}O_2$ and $PbPd_{0.9}Gd_{0.1}O_2$. (a) and (b) present the intensity and log intensity as a function of 2 theta, respectively.

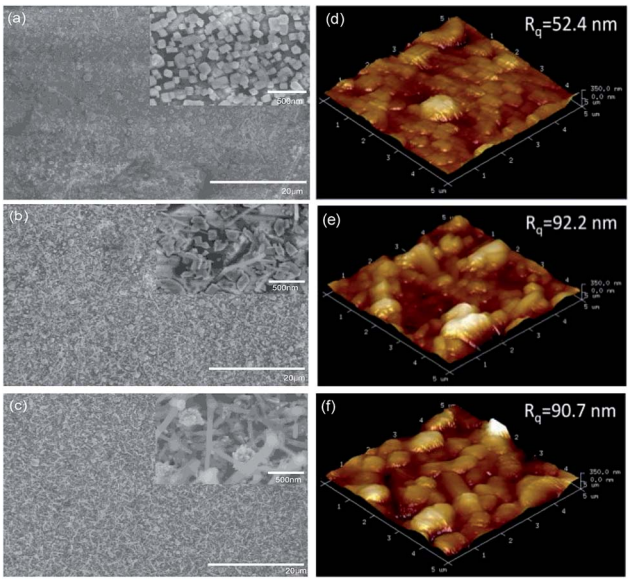

Fig. 2 SEM surface images and AFM surface morphologies of $PbPdO_2$ (a) and (d), $PbPd_{0.9}V_{0.1}O_2$ (b) and (e) and $PbPd_{0.9}Gd_{0.1}O_2$ (c) and (f).

deposition of the sample on the MgO substrate can lead to the shift of the diffraction peak (111) in the high angle direction of $PbPdO_2$. Therefore, the diffraction peak at 26.35° corresponds to the (111) diffraction peak of $PbPdO_2$. It is obvious that $PbPdO_2$, $PbPd_{0.9}V_{0.1}O_2$ and $PbPd_{0.9}Gd_{0.1}O_2$ films all grow along the (002) crystal face. So far, only $PbPdO_2$ and $PbPd_{0.75}Co_{0.25}O_2$ films with (112) crystal surface preferred growth were reported by Wang *et al.*[4] Here, (112) should be considered to be (002) according to XRD formula.

Fig. 2(a)–(f) shows the SEM images and AFM surface morphologies of $PbPdO_2$, $PbPd_{0.9}V_{0.1}O_2$, $PbPd_{0.9}Gd_{0.1}O_2$ thin films, respectively. Fig. 3(a), (b) and (c) show the EDS spectra of $PbPdO_2$, $PbPd_{0.9}V_{0.1}O_2$, $PbPd_{0.9}Gd_{0.1}O_2$ thin films, respectively. From Fig. 2(a), it can be found that the $PbPdO_2$ thin film is composed of nanoparticles with a particle size of about 100 nm and the $PbPd_{0.9}V_{0.1}O_2$ film contains many bar-like structures with width of 100–150 nm in Fig. 2(b). Moreover, Gd doping changes obviously the morphologies of the samples, and a lot of rod-like structures with the length of about 500 nm and width of about 100 nm are observed in Fig. 2(c). Moreover, from the surface morphologies in Fig. 2(d)–(f), the values of the surface roughness (R_q) are 52.4 nm, 92.2 nm and 90.7 nm for $PbPdO_2$, $PbPd_{0.9}V_{0.1}O_2$, $PbPd_{0.9}Gd_{0.1}O_2$ thin films, which is consistent with the observed results from SEM. The sizes of $PbPdO_2$, $PbPd_{0.9}V_{0.1}O_2$ and $PbPd_{0.9}Gd_{0.1}O_2$ thin films prepared by PLD technique are larger than those prepared by sol–gel spin coating.[5,12] From the EDS measured results in Fig. 3, it is obtained that the atomic ratio of Pb : Pd is 0.81 : 1.00 for $PbPdO_2$; Pb : Pd : V atomic ratio is 0.60 : 1.00 : 0.18 for $PbPd_{0.9}V_{0.1}O_2$; the atomic ratio of Pb : Pd : Gd is 0.57 : 1.00 : 0.18 for $PbPd_{0.9}Gd_{0.1}O_2$. It should specially be noticed that the Mg signal in the EDS spectra is from the MgO substrate. From the measured results, we can deduce that there exist Pb vacancies in the three samples, which may be caused by the volatilization of Pb during

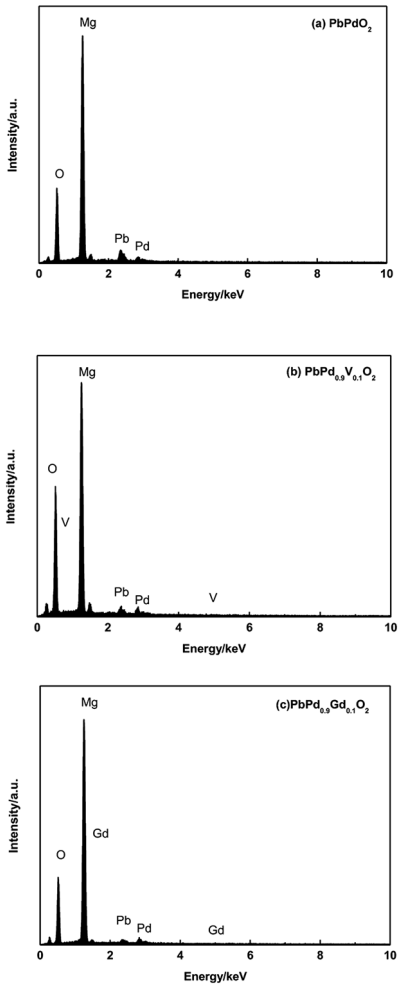

Fig. 3 EDS spectra of $PbPdO_2$ (a), $PbPd_{0.9}V_{0.1}O_2$ (b) and $PbPd_{0.9}Gd_{0.1}O_2$ (c).

the heating process. And the percentage of Pb vacancy in the samples also is changed due to the role of different ions. The measured results indicate that the percentage of Pb vacancy in $PbPdO_2$ is the lowest, and the percentage of Pb vacancy in $PbPd_{0.9}Gd_{0.1}O_2$ is the highest.

Fig. 4(a), (b) and (c) shows the XPS images of Pb 4f in $PbPdO_2$, $PbPd_{0.9}V_{0.1}O_2$ and $PbPd_{0.9}Gd_{0.1}O_2$ films, respectively. From the figures, it is found that the XPS spectra of Pb 4f for three films can be divided into two pairs of characteristic peaks corresponding to Pb $4f_{5/2}$ and Pb $4f_{7/2}$, which is similarly to previous studied results.[13] From Fig. 4(a), two pairs of characteristic peaks are described as following: main peaks (136.55 eV, 141.49 eV), and satellite peaks (137.50 eV, 142.20 eV); from Fig. 4(b), two pairs of characteristic peaks are described as following: main peaks (137.22 eV, 142.07 eV), and satellite peaks (138.05 eV, 142.88 eV); from Fig. 4(c), two pairs of characteristic peaks are described as following: main peaks (136.87 eV, 141.65 eV), and satellite peaks (137.75 eV, 142.50 eV). Clearly, with doping V and Gd, the sites and intensities of two pairs of peaks are changed, which means that doping has important role on ion vacancy and valence. The main peaks can be attributed to the lattice Pb of the samples, and the satellite peaks can be

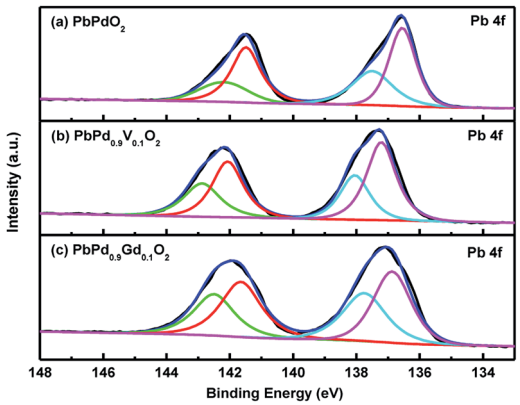

Fig. 4 XPS spectra of Pb in $PbPdO_2$ (a), $PbPd_{0.9}V_{0.1}O_2$ (b) and $PbPd_{0.9}Gd_{0.1}O_2$ (c).

attributed to Pb vacancies.[11] Moreover, the areas of main and satellite peaks for Pb $4f_{5/2}$ and Pb $4f_{7/2}$ in Fig. 4 were calculated. The calculated results indicate that the average area ratio of satellite peaks to total spectra (satellite + main peaks) are about 37.65%, 38.28% and 43.7% for Fig. 4(a), (b) and (c), respectively. Thus, it is obtained that Pb vacancies are about 37.65%, 38.28% and 43.7% for $PbPdO_2$, $PbPd_{0.9}V_{0.1}O_2$ and $PbPd_{0.9}Gd_{0.1}O_2$ films, respectively. The above results are consistent with the results of EDS.

Fig. 5(a), (b) and (c) shows Pd 3d XPS images for $PbPdO_2$, $PbPd_{0.9}V_{0.1}O_2$ and $PbPd_{0.9}Gd_{0.1}O_2$ thin films, respectively. From the figure, it is found that, both peaks for Pd 3d are symmetric and centered at around 336.28 eV and 341.59 eV for $PbPdO_2$, around 336.09 eV and 341.51 eV for $PbPd_{0.9}V_{0.1}O_2$, and around 336.10 eV and 341.51 eV for $PbPd_{0.9}Gd_{0.1}O_2$, respectively. The two peaks stand for Pd $3d_{5/2}$ and Pd $3d_{3/2}$, which can be attributed to the formation of Pd^{2+}.[13,18,19]

Fig. 6(a), (b) and (c) shows the XPS spectra of O 1s in $PbPdO_2$, $PbPd_{0.9}V_{0.1}O_2$ and $PbPd_{0.9}Gd_{0.1}O_2$ films, respectively. From the figure, it can be seen that every O 1s spectrum can be divided into three peaks with one main peak I at about 528.93–529.39 eV and two satellite peaks II and III at about 530.80–531.01 eV and 532.83–533.80 eV. Moreover, the sites of main peak and satellite

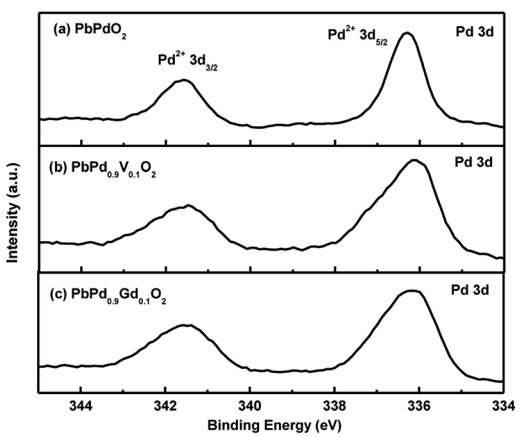

Fig. 5 XPS spectra of Pd of $PbPdO_2$ (a), $PbPd_{0.9}V_{0.1}O_2$ (b) and $PbPd_{0.9}Gd_{0.1}O_2$ (c).

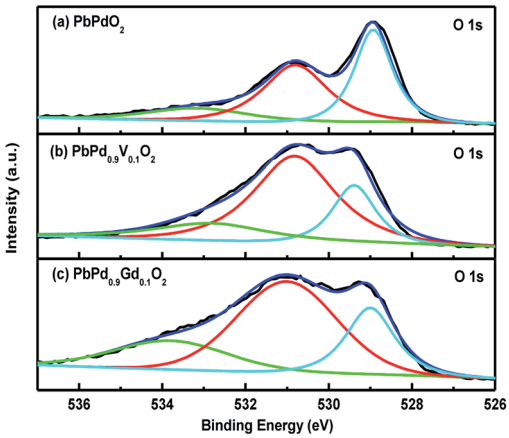

Fig. 6 XPS spectra of O 1s in $PbPdO_2$ (a), $PbPd_{0.9}V_{0.1}O_2$ (b) and $PbPd_{0.9}Gd_{0.1}O_2$ (c).

peaks are evidently influenced by V and Gd dopants. For $PbPdO_2$, $PbPd_{0.9}V_{0.1}O_2$ and $PbPd_{0.9}Gd_{0.1}O_2$ films, the main peak can be attributed to the lattice O in $PbPdO_2$, and the satellite peaks can be attributed to the oxygen and hydroxyl absorption on the surface of the sample.[20,21] In particular, the peak III at about 532.83–533.8 eV should be related to the Pb vacancy, which can be explained as follows: since the Pb vacancy is generated, the valence of Pb is changed from +2 to +0, which makes the excess oxygen oxidized to O^{1-}. As a result, O^{1-} will absorb hydroxyl and CO_2. Thus, the sample surface will be exposed in the atmosphere to absorb the hydroxyl and CO_2.[11] Compared with the doped samples, peak area percentage of II and III for the undoped sample is lowest. Thus, the content of Pb vacancies in undoped $PbPdO_2$ is lowest. It is reasonable to deduce that ion doping can increase surface absorbed oxygen and Pb vacancy. V and Gd dopants increase the content of Pb vacancies. Especially, Gd doping makes $PbPdO_2$ to produce most Pb vacancies. These results are consistent with the EDS those above.

Fig. 7(a) and (b) shows the XPS images of V and Gd in $PbPd_{0.9}V_{0.1}O_2$ and $PbPd_{0.9}Gd_{0.1}O_2$ films, respectively. From the Fig. 7(a), it can be seen that, two peaks at 515.70 eV and 516.80 eV should be corresponding to V^{4+} $2p_{3/2}$ and V^{5+} $2p_{3/2}$, respectively.[22–24] V^{4+} and V^{5+} ions coexist in the V doping TiO_2 has also been reported.[25] At the same time, one can notices that the two peaks of Gd at about of 1186.86 eV and 1220.86 eV should be corresponding to Gd^{3+} $3d_{5/2}$ and Gd^{3+} $3d_{3/2}$.[26,27]

Fig. 8(a), (b) and (c) show the *M–H* hysteresis loops for $PbPdO_2$, $PbPd_{0.9}V_{0.1}O_2$ and $PbPd_{0.9}Gd_{0.1}O_2$ at room temperature, respectively. From Fig. 8, it is found that three samples have all ferromagnetism at room temperature. The saturation magnetization of $PbPdO_2$, $PbPd_{0.9}V_{0.1}O_2$ and $PbPd_{0.9}Gd_{0.1}O_2$ were about 2.0 emu cm^{-3}, 5.0 emu cm^{-3} and 8.0 emu cm^{-3}, respectively. Obviously, V and Gd dopants improve magnetic moment of $PbPdO_2$, and enhancing effect of Gd dopant is largest. The source of magnetism is generally related to its defects, the carrier concentration, and the valence of the dopant ions for metal oxides.[28–30] Although, there exist very little impurity PdO and Gd_2O_3 phases in $PbPd_{0.9}V_{0.1}O_2$ and

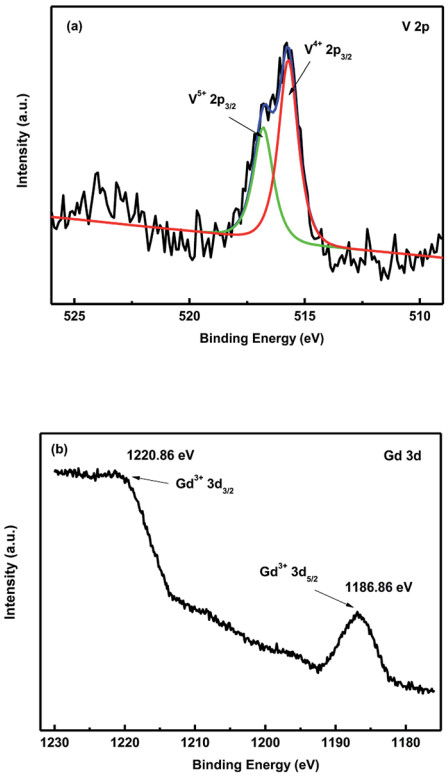

Fig. 7 XPS spectrum of (a) V 2p and (b) Gd 3d.

$PbPd_{0.9}Gd_{0.1}O_2$, these impurity phases do not contribute to ferromagnetism. Based on the above EDS and XPS measured results, one can notice that, the Pb vacancy, Pd^{2+} and O^{1-} exist in $PbPdO_2$. In theory, the effective spin magnetic moment of Pd^{2+} is zero. The magnetism of $PbPdO_2$ film should result from O^{1-}. Here, O^{1-} is produced due to the presence of Pb vacancies, and $2p^5$ in O^{1-} will lead to $1\mu_B$ effect magnetic moment. Moreover, the valence states of V and Gd ions were confirmed to be V^{4+}, V^{5+} and Gd^{3+} by XPS. For $PbPd_{0.9}V_{0.1}O_2$, V^{4+} can contribute $1\mu_B$ magnetic moment and V^{5+} makes no contribution. Therefore, the enhanced magnetism results from V doping. By contrast, Gd^{3+} can contribute $7\mu_B$ magnetic moment. Thus, Gd doping increases evidently the magnetism of

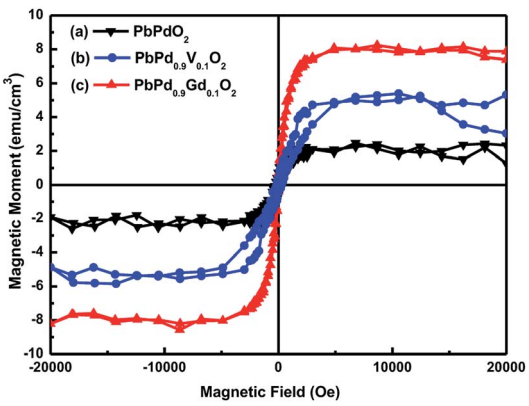

Fig. 8 M–H curves at room temperature of $PbPdO_2$ (a), $PbPd_{0.9}V_{0.1}O_2$ (b) and $PbPd_{0.9}Gd_{0.1}O_2$ (c).

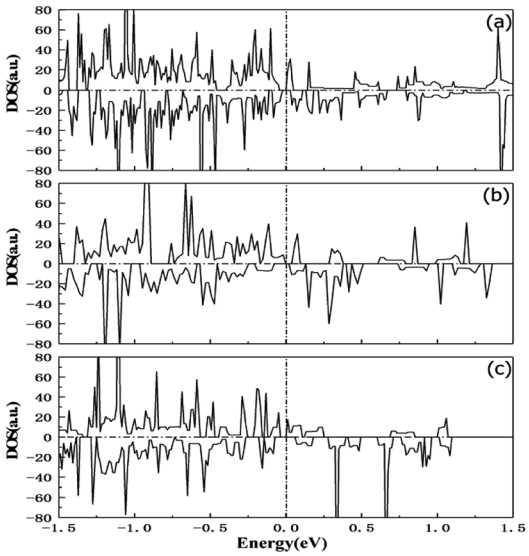

Fig. 9 The calculated spin DOSs of $PbPdO_2$ (a), $PbPd_{0.9}V_{0.1}O_2$ (b) and $PbPd_{0.9}Gd_{0.1}O_2$ (c).

$PbPd_{0.9}Gd_{0.1}O_2$. Fig. 9 shows the calculated spin DOSs of $PbPdO_2$, $PbPd_{0.9}V_{0.1}O_2$ and $PbPd_{0.9}Gd_{0.1}O_2$ with Pb vacancy. The calculated results indicate that, the magnetic moment of $PbPdO_2$ with Pb vacancy is $2.8\mu_B$, as shown in Fig. 9(a). As seen in Fig. 9(b) and (c), V dopant makes the magnetic moment to enhance to $6.5\mu_B$, and further Gd doping leads to the largest magnetic moment with $12.3\mu_B$. The doping role of the above magnetic moments explains well the experimental results in Fig. 8.

Fig. 10(a)–(c) shows the magnetization as a function of the temperature under zero-field cooling (ZFC) and field cooling (FC) for $PbPdO_2$, $PbPd_{0.9}V_{0.1}O_2$ and $PbPd_{0.9}Gd_{0.1}O_2$ thin films. As the temperature is changed from 370 K to 70 K, the ZFC and FC curves gradually separated. As the temperature is larger about 375 K, the FC and ZFC curves tended to coincide, and the crosspoint is named as blocking temperature. The evident deviation between the FC and ZFC curves indicates that superparamagnetism and ferromagnetism can coexist $PbPdO_2$, $PbPd_{0.9}V_{0.1}O_2$ and $PbPd_{0.9}Gd_{0.1}O_2$ thin films. These results are consistent with the previous report.[5]

Fig. 11 exhibits the temperature dependence of the DC electrical resistivity (ρ). It can be seen from the figure that the resistivities of $PbPdO_2$, $PbPd_{0.9}V_{0.1}O_2$ and $PbPd_{0.9}Gd_{0.1}O_2$ at room temperature are 0.179 Ω cm, 0.389 Ω cm and 0.143 Ω cm, respectively. Compared with the bulk resistivity,[3] these values become less. In addition, it is found that the resistivity of $PbPd_{0.9}V_{0.1}O_2$ is larger than that of $PbPdO_2$, and the resistivity of $PbPd_{0.9}Gd_{0.1}O_2$ is smaller than that of $PbPdO_2$. This indicates that different ion doping has a significant effect on the physical properties of $PbPdO_2$. To analyze the resistivity change produced by ion doping, the carrier densities and mobilities at room temperature for three films were measured, and the results are as following: for $PbPdO_2$, the hole-type carrier density and mobility is 5.56×10^{17} cm^{-3} and 2.22×10^4 cm^2 V^{-1} s^{-1}, respectively; for $PbPd_{0.9}V_{0.1}O_2$, they are 1.0×10^{17} cm^{-3} and 20.2×10^4 cm^2 V^{-1} s^{-1}; for $PbPd_{0.9}Gd_{0.1}O_2$, they are 26.9 ×

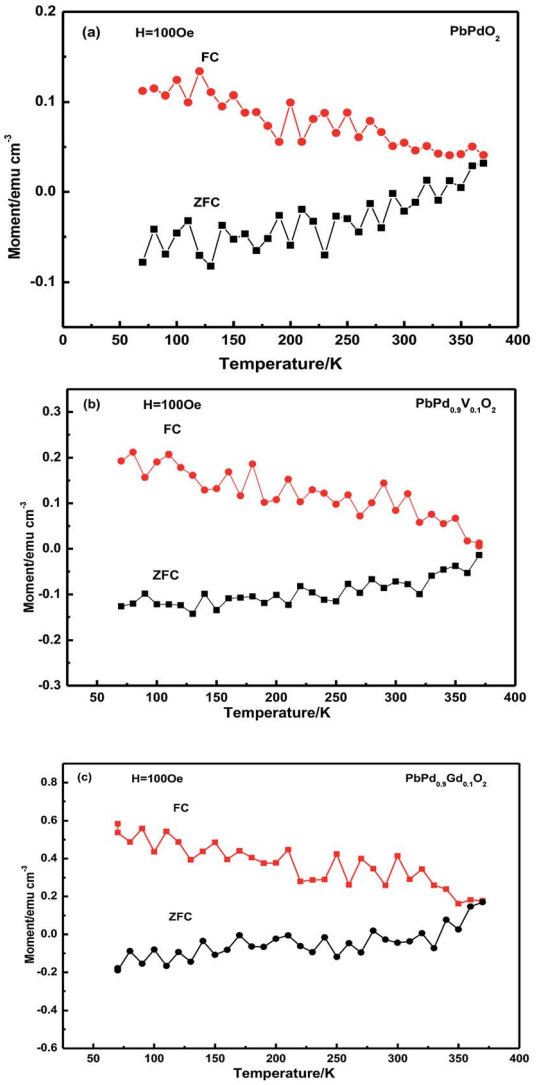

Fig. 10 ZFC–FC M–T curves of $PbPdO_2$ (a), $PbPd_{0.9}V_{0.1}O_2$ (b) and $PbPd_{0.9}Gd_{0.1}O_2$ (c) thin films.

10^{17} cm^{-3} and 7.1×10^4 cm^2 V^{-1} s^{-1}, respectively. Obviously, the resistivity change produced by ion doping can be explained by difference of the carrier density. To clarify the role of vacancy and dopant on the resistivity, we have also carried out first-principles calculations. From the calculated spin-polarized DOSs of $PbPdO_2$, $PbPd_{0.9}V_{0.1}O_2$ and $PbPd_{0.9}Gd_{0.1}O_2$ in Fig. 9, one can find that V and Gd dopants have clear role on the band gap. From Fig. 9(a), the presence of Pb vacancies results in a band gap of 0.028 eV in $PbPdO_2$. After the further doping of Gd and V atoms, we found distinct effects on the band gap: the introduction of Gd^{3+} reduces the band gap to 0.019 eV, while the doping of $V^{4+,5+}$ increases the band gap to 0.036 eV. The above calculated results reveal well the variation of electrical resistivity for three samples as shown in Fig. 11.

The electron transport in $PbPdO_2$ is controlled by hole carriers through the Pd–O hybridization, and the doping of Gd ions can make the Pd–O hybrid stronger, while the doping of V ions weaken the Pd–O hybridization. Therefore, ion doping

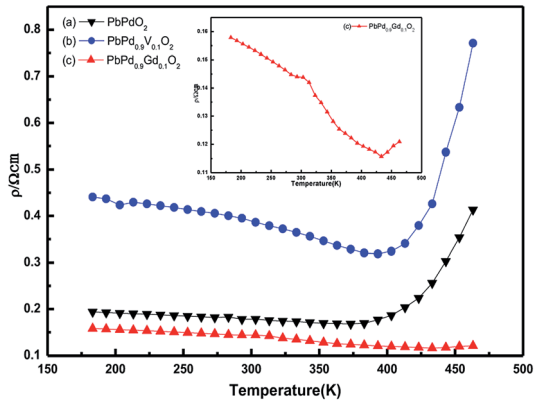

Fig. 11 Temperature dependence of DC electrical resistivity for $PbPdO_2$, $PbPd_{0.9}V_{0.1}O_2$ and $PbPd_{0.9}Gd_{0.1}O_2$ thin films. The inset shows the magnified temperature dependence of resistivity of $PbPd_{0.9}Gd_{0.1}O_2$ thin film.

significantly changes the conductivity of the sample. In addition, it is found that there is a significant insulator–metal transition temperature in the samples. The insulator–metal transition temperatures for $PbPdO_2$, $PbPd_{0.9}V_{0.1}O_2$ and $PbPd_{0.9}Gd_{0.1}O_2$ are respectively about 385 K, 390 K, 430 K, which is much higher than previous experimental reports.[2,4] Significant differences in T_{MI} may be related to microstructural differences arising from different preparation conditions.

Conclusions

$PbPdO_2$, $PbPd_{0.9}V_{0.1}O_2$ of $PbPd_{0.9}Gd_{0.1}O_2$ films with the preferred orientation of (002) have been synthesized by PLD technique. The particle size and surface roughness of three films were obtained by SEM and AFM measurements. Moreover, the valence states for Pb, Pd, O, Gd and V ions were found to be 2+, 2+, 2−, 3+ and the mixed 4+ and 5+, respectively. Meanwhile, it is found that three samples have Pb vacancies and room temperature ferromagnetism. The saturation magnetization of $PbPdO_2$, $PbPd_{0.9}V_{0.1}O_2$ and $PbPd_{0.9}Gd_{0.1}O_2$ were found to be about 2.0 emu cm^{-3}, 5.0 emu cm^{-3} and 8.0 emu cm^{-3}, respectively. Moreover, the temperature dependence of resistivity indicates that, the electrical resistivity is enhanced by V ion substitution, but being weakened by Gd ion substitution. Significant insulator–metal transition temperatures were also observed. Finally, based on the calculated spin DOSs of $PbPdO_2$, $PbPd_{0.9}V_{0.1}O_2$ and $PbPd_{0.9}Gd_{0.1}O_2$ with Pb vacancy, the magnetic origin of three samples, and V (Gd) doping roles on the electrical and magnetic properties can be explained well.

Conflicts of interest

There are no conflicts to declare.

Acknowledgements

This work is supported by the National Science Foundation of China (61574037, 61404029, 11404058, 11274064); Natural

Science Foundations of Fujian Province of China (Grant No. 2017J06001).

Notes and references

1 X.-L. Wang, S. X. Dou and C. Zhang, *NPG Asia Mater.*, 2010, **2**(1), 31–38.
2 T. C. Ozawa, T. Taniguchi, Y. Nagata, Y. Noro, T. Naka and A. Matsushita, *J. Alloys Compd.*, 2005, **388**, 1–5.
3 X. L. Wang, *Phys. Rev. Lett.*, 2008, **100**, 3136–3140.
4 X. L. Wang, G. Peleckis, C. Zhang, H. Kimura and S. X. Dou, *Adv. Mater.*, 2009, **21**, 2196–2199.
5 H. L. Su, S. Y. Huang, Y. F. Chiang, J. C. A. Huang, C. C. Kuo, Y. W. Du, Y. C. Wu and R. Z. Zuo, *Appl. Phys. Lett.*, 2011, **99**, 102508.
6 S. M. Choo, K. J. Lee, S. M. Park, G. S. Park and M. H. Jung, *J. Appl. Phys.*, 2013, **113**, 014904.
7 S. M. Choo, K. J. Lee, S. M. Park, J. B. Yoon, G. S. Park, C.-Y. You and M. H. Jung, *Appl. Phys. Lett.*, 2015, **106**, 172404.
8 K. J. Lee, S. M. Choo, J. B. Yoon, K. M. Song, Y. Saiga, C.-Y. You, N. Hur, S. I. Lee, T. Takabatake and M. H. Jung, *J. Appl. Phys.*, 2010, **107**, 09C306.
9 K. J. Lee, S. M. Choo and M. H. Jung, *Appl. Phys. Lett.*, 2015, **106**, 072406.
10 K. J. Lee, S. M. Choo, Y. Saiga, T. Takabatake and M. H. Jung, *J. Appl. Phys.*, 2011, **109**, 07C316.
11 X. Chen, Y. Chen, Y. M. Yang, H. Jia, J. M. Zhang, S. Y. Chen and Z. G. Huang, *Ceram. Int.*, 2017, **43**, 10428–10433.
12 J. Liu, C. Mei, P. Y. Chuang, T. T. Song, F. L. Tang, H. L. Su, J. C. A. Huang and Y. C. Wu, *Ceram. Int.*, 2016, **42**, 15762–15766.
13 F. L. Tang, J. Liu, C. Mei, S. Y. Huang, T. T. Song, H. L. Su, M. K. Lee, Y. C. Wu and J. C. A. Huang, *RSC Adv.*, 2016, **6**, 37522–37529.
14 G. Kresse and J. Hafner, *Phys. Rev. B: Condens. Matter Mater. Phys.*, 1993, **48**, 13115–13118; G. Kresse and J. Furthmüller, *Phys. Rev. B: Condens. Matter Mater. Phys.*, 1996, **54**, 11169.
15 P. E. Blöchl, *Phys. Rev. B: Condens. Matter Mater. Phys.*, 1994, **50**, 17953.
16 G. Kresse and J. Furthmüller, *Comput. Mater. Sci.*, 1996, **6**, 15.
17 J. P. Perdew, K. Burke and M. Ernzerhof, *Phys. Rev. Lett.*, 1996, **77**, 3865.
18 K. C. Lee, Y. J. Chiang, Y. C. Lin and F. M. Pan, *Sens. Actuators, B*, 2016, **226**, 457–464.
19 M. Brun, A. Berthet and J. C. Bertolini, *J. Electron Spectrosc. Relat. Phenom.*, 1999, **104**, 55–60.
20 H. Q. Zhao, J. Wang, L. X. Zhang, Y. C. Rong, J. Chen, K. Ibrahimb and X. R. Xing, *Dalton Trans.*, 2013, **42**, 10358–10364.
21 S. Takatani, H. Miki, K. Kushida-Abdelghafar and K. Torii, *J. Appl. Phys.*, 1999, **85**, 7784–7791.
22 J. Xu, C. X. Qin, Y. L. Huang, Y. R. Wang, L. Qin and H. J. Seo, *Appl. Surf. Sci.*, 2017, **396**, 1403–1410.
23 R. Larsson, B. Folkesson and G. Schoen, *Chem. Scr.*, 1973, **3**, 88.
24 V. I. Nefedov, M. N. Firsov and I. S. Shaplygin, *J. Electron Spectrosc. Relat. Phenom.*, 1982, **26**, 65.
25 F. Z. Ren, H. Y. Li, Y. X. Wang and J. J. Yang, *Appl. Catal., B*, 2015, **176**, 160–172.
26 Y. Uwamino, Y. Ishizuka and H. Yamatera, *J. Electron Spectrosc. Relat. Phenom.*, 1984, **34**, 69.
27 D. Raiser and J. P. J. Deville, *J. Electron Spectrosc. Relat. Phenom.*, 1991, **57**, 91.
28 A. Sundaresan and C. N. R. Rao, *Nano Today*, 2009, **4**(1), 96–106.
29 S. B. Ogale, *Adv. Mater.*, 2010, **22**(29), 3125–3155.
30 T. Dietl, *Nat. Mater.*, 2010, **9**(12), 965–974.